

We are IntechOpen, the world's leading publisher of Open Access books Built by scientists, for scientists

4,800

Open access books available

122,000

International authors and editors

135M

Downloads

Our authors are among the

154

Countries delivered to

TOP 1%

most cited scientists

12.2%

Contributors from top 500 universities



WEB OF SCIENCE™

Selection of our books indexed in the Book Citation Index
in Web of Science™ Core Collection (BKCI)

Interested in publishing with us?
Contact book.department@intechopen.com

Numbers displayed above are based on latest data collected.
For more information visit www.intechopen.com



Information Extraction and Despeckling of SAR Images with Second Generation of Wavelet Transform

Matej Kseneman¹ and Dušan Gleich²

¹Margento R&D d.o.o.,

²University of Maribor, Faculty of Electrical Engineering and Computer Science,
Slovenia

1. Introduction

Synthetic Aperture Radar (SAR) technology is mainly used to obtain high-resolution images of ground areas in resolutions even less than meter. SAR is even capable of imaging a wide area of terrain and from two and more images it is possible to reconstruct a 3D digital elevation model of ground terrain. Good thing about SAR is an all-weather operation and possibility to capture images under various inclination angles. Because digital images are usually corrupted by noise that arises from an imaging device, there is always a need for a good filtering algorithm to remove all disturbances, thus enabling more information extraction. The SAR images are corrupted by a noise called speckle, which makes the interpretation of SAR images very difficult. The goal of removing speckles from the SAR image is to represent a noise-free image and preserve all important features of the SAR image, as for example edges, textures, region borders, etc.

Many different techniques for SAR image despeckling have been proposed over the past few years. Speckle is a noise-like characteristic of SAR images and it is a multiplicative nature, if the intensity or amplitude image is observed. The despeckling can be performed in the image or in the frequency domain. The well-known despeckling filters are Lee (Lee, 1980), Kuan (Kuan et al., 1985), and Frost (Frost et al., 1982). Lee and Kuan filters can be considered as an adaptive mean filters, meanwhile the Frost filter can be considered as a mean adaptive weighted filter. The Bayesian filters are based on the Bayesian theorem, which defines a posterior probability by using a prior, likelihood and evidence probability density functions (pdf). The solution for noise-free image is found by a maximum a posteriori (MAP) estimate. The MAP estimate of a noise-free image was proposed in (Walessa & Datcu, 2000), where the noise-free image was approximated by a Gauss-Markov random field prior and the noise was modeled with Gamma pdf. Model-based despeckling and information extraction is one of the promising techniques of SAR image denoising and scene interpretation. The wavelet-based despeckling algorithms have been proposed in (Dai et al., 2004), (Argenti & Alparone, 2002), and (Foucher et al., 2001). The second-generation wavelets Chirplet (Cui & Wong, 2006), Contourlet (Chuna et al., 2006), Bandelet (Le Pennec & Mallat, Apr 2005) have appeared over the past few years.

First transform we used is so called Bandelet transform (Le Pennec & Mallat, Dec 2005), which further divides wavelet subbands into smaller subbands using a rate distortion optimization that enables removing redundancy in wavelet transformation. Bandelets (Le Pennec & Mallat, Dec 2005) contain anisotropic wavelets which combine redundancy in the geometric flow of an image corresponding to local directions of its grey levels. With this geometric flow wavelet warping represents a vector field with indication of regularity along edges. Bandelet decomposition is constructed in much the same way as wavelet with use of dyadic squares containing information about bandelet coefficients (parameterized geometric flow) and segmentation (Le Pennec & Mallat, Apr 2005). These squares summarize geometry by local clustering of similar directional vectors. A Bandelet transform can be viewed as an adaptive wavelet basis transform, which is warped according to local direction.

Bandelet transform is therefore capable to separate two different surface areas with different curvatures, which are then decomposed into optimal estimations of regularity direction (Le Pennec & Mallat, Apr 2005). The geometry itself is obtained with regularity flow estimation. Fig. 1 shows an example of directions acquired with bandelet transform. The computational complexity of this transform is much higher as in the case of the classical dyadic decomposition.

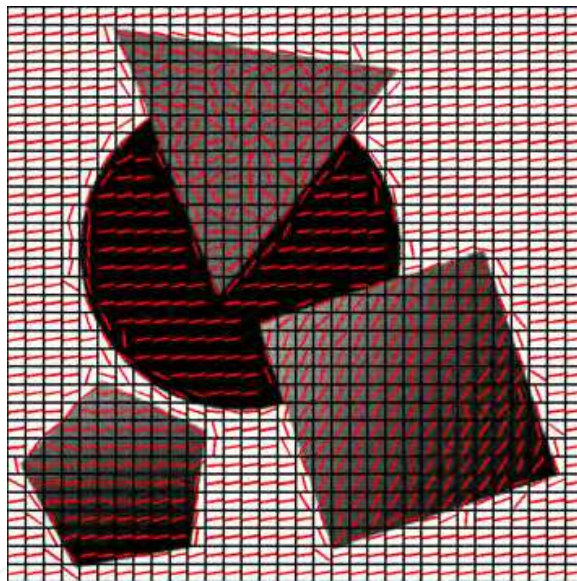


Fig. 1. Directions obtained by bandelet transform

The contourlet transform (Do & Vetterli, 2005) is organized a little bit differently, because this transform is directly constructed in a discrete space. Thus, contourlet does not need to be transformed from continuous time-space domain. In order to capture as much as possible directional information a 2D directional filter bank is used in contourlet transform (Do & Vetterli, 2005). Directional filter bank is represented with k -binary tree which decomposes original image into $2k$ bands. These directional filter banks have a flaw mainly because they are designed to capture a direction, which is mainly done in high frequency spectrum of the input image, therefore low frequencies are obstructed. Low frequencies can easily penetrate into several different directional subbands, thus corrupting the transformation subbands. To solve this problem a multiscale decomposition is created with directional decomposition with the help of Laplacian pyramid as a low frequency filter. Laplacian pyramid throughput

is a band-pass image which is then led to directional filter bank where a directionality of an image is captured. This scheme can be further applied on a coarser image and thus an iterative scheme can be achieved. It can be concluded that applying iterative contourlet scheme derives to directional subbands in a presence of multiple different scales.

For the despeckling of TerraSAR-X (Wikipedia, 2011) images we used a model based approach, which is supported by first order Bayesian inference. After applying transforms to images a general Gaussian distribution appears in wavelet domain. In this wavelet domain we get subbands different in scales and frequency. The subbands in the wavelet domain have Gaussian distribution and therefore the general Gaussian model is used for a prior density function (pdf). The likelihood pdf is modeled using Gaussian pdf in both, bandelet and contourlet transforms. The despeckling using contourlet (Li et al., 2006) and bandelet (Sveinsson et al., 2008) transforms showed superior despeckling results for SAR images comparing with the wavelet based methods. The model based despeckling mainly depends on chosen models. The image and noise models in the wavelet domain are well defined with presented results in (Argenti & Alparone, 2002), (Gleich & Datcu, 2006) and usually noise-free image is computed using maximum a posteriori estimate.

The despeckling methods were tested using synthetic and real TerraSAR-X data, which were captured in the high resolution spotlight mode. The experimental results showed that the best despeckling method for synthetic images is bandelet transform, because contourlet transform produces artifacts in the homogenous areas. The ratio images between original and despeckled images were examined in order to show estimation of speckle noise, edge and texture preservation using bandelet and contourlet transform. The contourlet transform produces artifacts in form of lines in both homogenous areas and edges.

2. Second generation wavelets

In this section a comparison between bandelets and contourlets is presented. Bandelets and contourlets are presented in great detail, including subbands creation and filter decomposition. These two denoising schemes are a foundation of later proposed model, which builds a denoising scheme on top of these two schemes yielding better denoising results.

2.1 Bandelets

Bandelets (Le Pennec & Mallat, Apr 2005), (Le Pennec & Mallat, Dec 2005) belong to a second generation of wavelet transforms and are composed of anisotropic wavelets, which are in fact a combination of geometric flow of an image corresponding to local directions of its gray levels. This geometric flow represents a regularity of a vector field along edges contained in the image. Typical example of this geometric flow can be seen on Fig. 1, where it can be observed that all directions are aligned to object's edges at the boundary of two different areas.

Edges inside an image are often hard to determine. First generation of bandelet transform uses the vector field (Le Pennec & Mallat, 2001), which determines image regularities and irregularities. Therefore bandelet coefficients represent geometric flow defined by polynomial function. This geometric flow consists of directions of variations in image grey levels, where linear geometric flow is preferred. Bandelet transform image is divided into

regions with corresponding vector fields, which describes directions of regularity inside a predefined neighborhood.

If the image intensity is uniformly regular in the neighborhood of a point, then this direction is not uniquely defined, and some form of global regularity is therefore imposed on the flow to specify it uniquely.

In literature it has been proven that the first generation of bandelets has minimum distortion for images whose edges correspond to geometric regularity. However, the first generation of bandelets is composed in continuous space, thus not being able to represent a multi-resolution of the geometric regularity. Thus, the second generation of bandelets (Le Pennec & Mallat, Apr 2005) was introduced, which is an orthogonal multiscale transform constructed directly in discrete domain. The bandelet transform first creates a composition of smaller images representing subbands, and then uses fast subband-filtering algorithms. For applications including speckle-noise removal, the geometric flow is optimized in a way that bandelet transform produces minimum distortion in reconstructed images. The decomposition on a bandelet basis is computed using a wavelet filter bank followed by adaptive geometric orthogonal filters, which require $O((\log_2 N)^3)$ operations.

The key parameters in bandelet transform are: the estimation of basis shapes, the partition of images, and the optimization of geometric flows (Yang et al., 2007). To represent image with as little as possible information, the complex edges must be divided into simpler smaller shapes so that linear geometric flows can represent them sufficiently. The image is commonly divided into smaller square regions that are being divided until there is only one contour inside a square region. It must be noted that the geometric regularity should be discrete, so dyadic decomposition by successive subdivisions of square regions into four smaller sub-squares of twice smaller width can be made. There is a defined maximum and minimum block size (Le Pennec & Mallat, Apr 2005), where the first division produces blocks of maximum size, while later iterations divide those blocks up until minimum size is reached. This partition result can be viewed as a quadtree, where each block is represented by its corresponding leaf in a tree. At each scale the resulting geometry is multiscale and calculated by a procedure that minimizes the Lagrangian cost function.

Implementation

The bandelet transform first computes the 2D wavelet transform of the input original image (Peyré & Mallat, Apr 2005). This transform is based on orthogonal or biorthogonal filter banks and results in four smaller images (children) containing low- and high-frequency components. By selecting a dyadic square and recursively splitting input wavelet image four new sub-squares are created. Further on geometric flow parameterization is performed in each of these sub-squares in every possible direction. Let us assume that each of these squares has a width of k pixels then the number of potential directions d is a little less than $2k^2$. The sampling location is then projected along potential direction and afterwards sorting the resulting 1D points is performed from left to right direction. These points define 1D discrete signal f_d (Le Pennec & Mallat, Apr 2005) which is later on transformed with 1D discrete wavelet transform. For a given user defined threshold T , the bandelet transform has to find the best available direction, which in fact produces the less approximation error. Best geometry is obtained by choosing best direction d that minimizes the Lagrangian

$$\mathcal{L}(f_d, R) = \|f_d - f_{dR}\|^2 + \lambda T^2 (R_G + R_B) \quad (1)$$

where f_{dR} is the recovered signal from quantized coefficients acquired by inverse 1D wavelet transform, R_G is the number of bits needed to code geometric parameter d , R_B is the number of bits needed to code the quantized coefficients and $\lambda = 3/28$ (Le Pennec & Mallat, Apr 2005).

When there are gathered all approximations over each individual dyadic square, the quadtree can be constructed. The algorithm starts with the smallest squares that represent a leaf in quadtree and initialize the cumulative Lagrangian of the sub-tree. Within these dyadic squares, a best bandelet approximation is obtained by minimizing a Lagrangian cost function (Le Pennec & Mallat, Dec 2005). Fig. 2 shows an example of denoising obtained with the bandelet transform including dyadic squares that indicate a progress of dyadic levels. This image is represented by indexing a dyadic level used in bandelet transform, where white indicates the first level and black the last level achieved.



Fig. 2. An example of image denoising using a bandelet transforms. a) Original image, b) Denoised image using a bandelet transforms, and c) Dyadic squares tree

2.2 Contourlets

Contourlet transform (Do & Vetterli, 2005) is also classified as a second generation wavelet transform for which a Fourier transform is not needed anymore. Main advantage of second generation wavelet transform over the first generation is a true discrete 2D transformation, which is able to capture geometry of an image, but the first generation wavelet transform does not perform very well on edge regions. This transformation therefore results in adaptive multi-resolution and directional image expansion using contour segments.

Best performance of wavelets is achieved in 1D case which is for example only one row of a 2D picture. Because pictures are not simply stacks of rows, discontinuities evolve along smooth regions. 2D wavelet transform thus captures edge points, but on the other hand the throughput on smooth regions is not quite as good anymore. Moreover wavelet transform can only capture a fraction of image directionality, which is clearly seen in Fig. 3 where wavelet transform needs a lot more subdivisions and information than a contourlet transform.

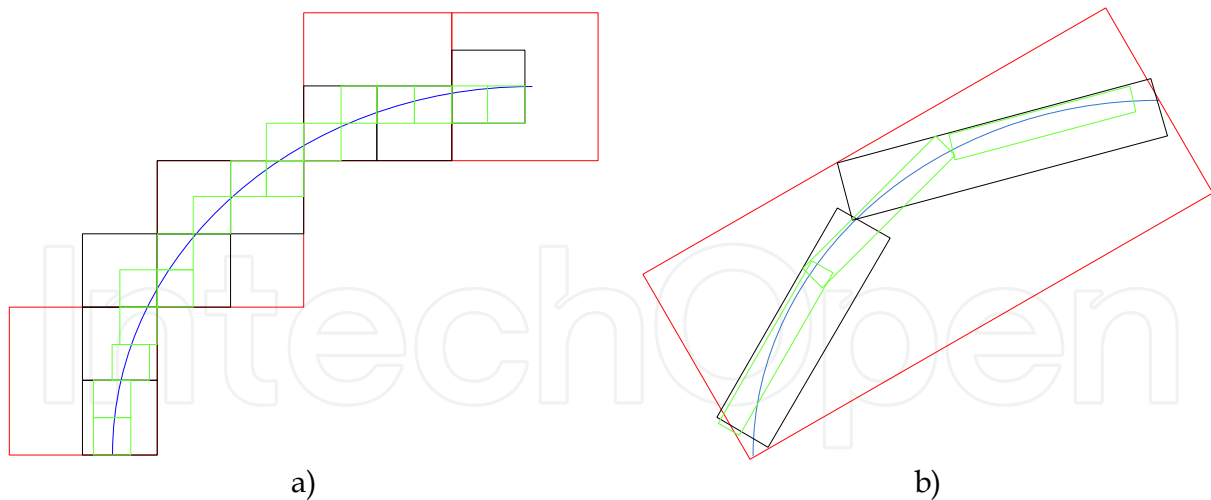


Fig. 3. a) Subdivision comparison between wavelet, and b) Contourlet transform

In order to capture as much as possible directional information a new type of filter bank has to be constructed. Thus a 2D directional filter bank (Bamberger & Smith, 1992) is used in Contourlet transform. Directional filter bank is represented by k -binary tree, which decomposes original image into 2^k subbands as represented in Fig. 4. The algorithm based on contourlet transform uses a simpler version of directional filter bank, where the first part is constructed from two-channel quincunx filter bank (Vetterli, 1984), while the second part is sampling and reordering operator. With this composition a frequency partition is achieved and also a perfect reconstruction is obtained. As shown in Fig. 6 one can obtain different 2D spectrum decompositions with appropriate combinations of aforementioned building blocks. Thus a k -level binary tree directional filter bank can be viewed as 2^k parallel channel filter bank with equivalent filters and its sampling matrices as shown in Fig. 5 (Do & Vetterli, 2005). In Fig. 5 D denotes an equivalent directional filter.

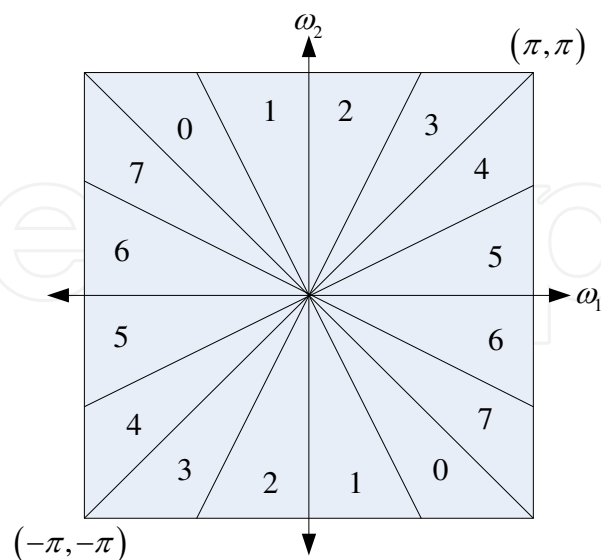


Fig. 4. Frequency partitioning where $k = 3$ and there are $2^3 = 8$ real wedge-shaped frequency bands. Subbands 0-3 correspond to the mostly horizontal directions, while subbands 4-7 correspond to mostly vertical directions

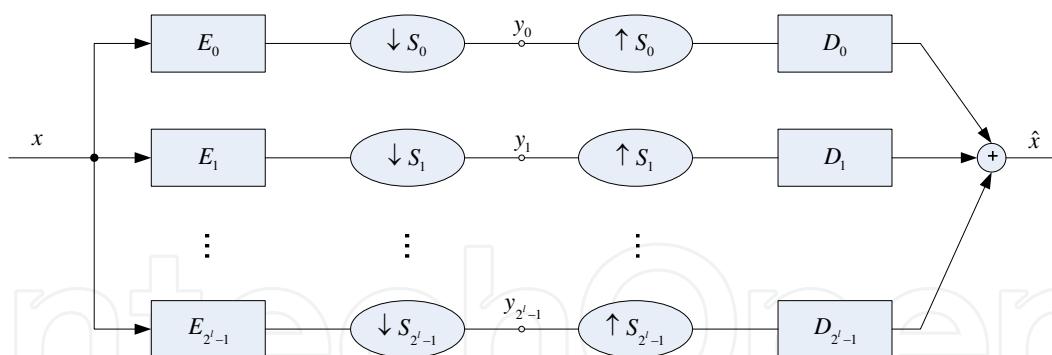


Fig. 5. The multichannel view of a k -level tree-structured directional filter bank

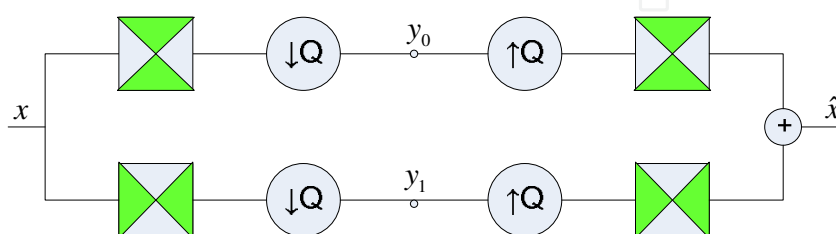


Fig. 6. 2D partition of spectrum using quincunx filter banks with fan filters. Darker shades represent the ideal frequency supports of each filter. Denotation Q represents a quincunx sampling matrix

These directional filter banks have a flaw mainly because they are designed to capture directions, which is mainly done in high frequency spectrum of the input image and thus low frequencies are obstructed. As Fig. 5 shows frequency partition a low frequencies can easily penetrate into several different directional subbands and therefore corrupt the transformation subbands. It is therefore wise to combine multiscale decomposition with directional decomposition with the help of Laplacian pyramid as a low frequency filter. Laplacian pyramid throughput is a bandpass image which is then led to directional filter bank where a directionality of the image is captured. This scheme can be further applied on a coarser image and thus an iterative scheme can be achieved. It can be concluded that applying iterative contourlet scheme derives to directional subbands in presence of multiple different scales, which is depicted in Fig. 7.

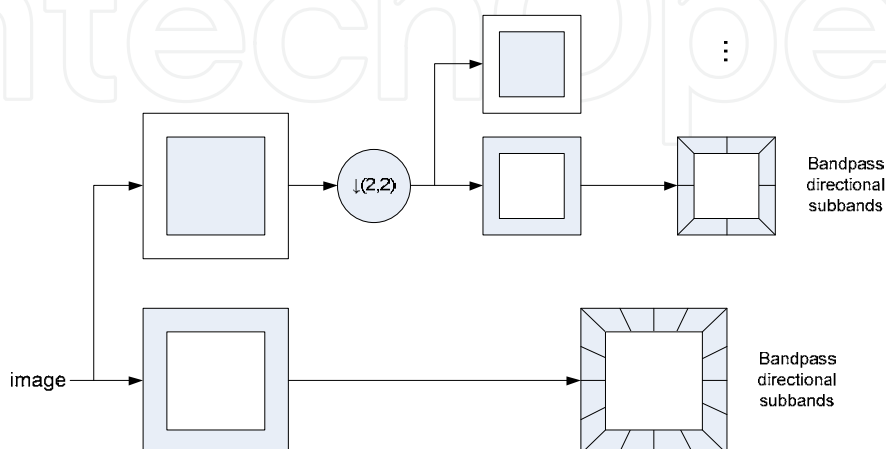


Fig. 7. Construction of contourlet filter bank

3. Bayesian inference incorporated into second generation wavelet transform

The first level of Bayesian inference is given by

$$p(x|y, \theta) = \frac{p(y|x, \theta)p(x|\theta)}{p(y|\theta)} \quad (2)$$

where y represents a noisy image, x represents a noise-reduced image, the θ 's are the model parameters, $p(y|x, \theta)$ denotes the conditional pdf called **likelihood**, $p(x|\theta)$ denotes **prior** pdf, and $p(y|\theta)$ represents **evidence** pdf. In Eq. (2), the evidence pdf does not play a role in the maximization over x , and therefore, the MAP estimator can be written by

$$\hat{x}(y) = \arg \max_x p(y|x, \theta)p(x|\theta) \quad (3)$$

where the likelihood and prior pdfs should be defined. The MAP estimator is an optimal estimator and minimizes the given cost function. The speckle noise in SAR images is modeled as multiplicative noise, i.e. $y = x \cdot z$, where z represents pure speckle noise. A multiplicative speckle noise can also be modeled using an additive signal-dependent model, as proposed in (Argenti & Alparone, 2002) $y = x \cdot z = x + x(z - 1) = x + n$, where n is a non-stationary signal-dependent additive noise equal to $x(z - 1)$.

Models describing texture parameters are widely used in SAR image despeckling (Walessa & Datcu, 2000). Let us model the image as generalized Gauss-Markov random fields (GGMRF) given by

$$p(x_s|\theta) = \frac{\nu\eta(\nu, \sigma_x)}{2\Gamma(1/\nu)} \exp\left\{-\left[\eta(\nu, \sigma_x)\left|x_s - \sum_{r \in \zeta_s} \theta_r (x_{s+r} + x_{s-r})\right|\right]^\nu\right\} \quad (4)$$

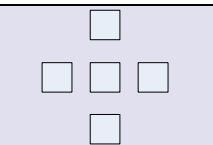
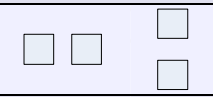
Neighborhood	
Cliques	
Parameters	θ_1 θ_2

Fig. 8. First order cliques

Let σ_x and θ_s define the GGMRF with a neighborhood set ζ_s . The MRF model characterizes the spatial statistical dependence of 2D data by a symmetric set called neighboring set. The expression $\sum \theta_r (x_{s+r} + x_{s-r})$ in Eq. (4) represents the sum of all the distinct cliques of neighboring pixel at a specific subband level. A clique is defined as a subset of sites neighboring the observed pixel, where every pair of sites is neighbors of each other. In this double site, cliques are used. A sum is performed over horizontal and vertical neighboring

pixels, for the first model order of the MRF. The neighbor set for a first model order is defined as $\zeta = \{(0, 1), (0, -1), (1, 0), (-1, 0)\}$, and can be seen in Fig. 8. Moreover, the neighbor set for a second model order is defined as $\zeta = \{(0, 1), (0, -1), (1, 0), (-1, 0), (1, 1), (-1, -1), (1, -1), (-1, 1)\}$. The MRF model is defined for the symmetric neighbor set; therefore, if $r \in \zeta_s$, then $-r \notin \zeta_s$, and ζ is defined as $\zeta = (r: r \in \zeta_s) \cup (-r: r \in \zeta_s)$. The parameter ν in (4) represents the shape parameter of the GGMRF, $\Gamma(\cdot)$ represents the Gamma function, and η is given by

$$\eta(\nu, \sigma_x) = \sigma_x^{-1} \sqrt{\frac{\Gamma(3/\nu)}{\Gamma(1/\nu)}} \quad (5)$$

A likelihood pdf is given by a Gaussian distribution

$$p(y_s | x_s) = \frac{1}{\sqrt{2\pi\sigma_n^2}} \exp\left(-\frac{(y_s - x_s)^2}{2\sigma_n^2}\right) \quad (6)$$

where σ_n^2 is a noise variance.

The noise variance σ_n^2 can be estimated using the results presented in (Argenti & Alparone, 2002), and is given by

$$\sigma_n^2 = \psi_l \mu_x^2 C_F^2 (1 + C_x^2) \quad (7)$$

where $\mu_x = E[x]$, and $E[x]$ denotes a mathematical expectation. C_x^2 is given by

$$C_x^2 = \frac{C_{Wy}^2 - \psi_l C_F^2}{\psi_l (1 + C_F^2)} \quad (8)$$

The normalized standard deviation of the noisy wavelet coefficient is given by $C_{Wy} = \sigma_{Wy} / \mu_y$, where σ_{Wy} is a standard deviation calculated within the wavelet domain, and μ_y is the mean value calculated in the spatial domain. C_F denotes the normalized standard deviation of the speckle noise. The parameter ψ_l is defined as a product of the coefficients from high-pass (g_k) and low-pass (h_k) filter used at the l -th level of the wavelet decomposition. If the wavelet coefficients of a diagonal detail are of interest, then the parameter ψ_l is given by

$$\psi_l = \left(\sum_k h_k^2\right)^2 \left(\sum_k g_k^2\right)^{2(l-1)} \quad (9)$$

Moreover, if the wavelet coefficients in the horizontal and vertical details are of interest, then the parameter ψ_l is given by

$$\psi_l = \left(\sum_k h_k^2\right) \left(\sum_k g_k^2\right)^{2l-1} \quad (10)$$

Since the random variable z of the speckle noise is normalized (i.e. $E[z] = 1$), the parameter C_F for intensity images is given by

$$C_F = 1/\sqrt{L} \quad (11)$$

while for the amplitude images the parameter C_F is given by

$$C_F = \sqrt{(4/\pi - 1)/L} \quad (12)$$

The parameter L represents the number of looks of the original SAR image. However, its value is unknown, thus an approximation has to be done, which is $L = \mu^2/\sigma^2$. The noise variance is then given by

$$\sigma_n^2 = \frac{C_F^2(\psi_l \mu_y^2 + \sigma_{W_y}^2)}{1 + C_F^2} \quad (13)$$

where $\mu_y = E[y]$. Noise-reduced variance can be computed using the results presented in the paper (Argenti & Alparone, 2002). Thus, noise-reduced the variance is given by

$$\sigma_x^2 = \psi_l \mu_x^2 C_x^2 \quad (14)$$

Where μ_x^2 is the mean value calculated within the wavelet domain over a predefined window size.

The MAP estimate using the GGMRF primarily defined in (4) and the likelihood defined in (6) is given by

$$-v\eta(v, \sigma_x) \left[\eta(v, \sigma_x) \left| x_s - \sum_{r \in \zeta_s} \theta_r (x_{s+r} + x_{s-r}) \right| \right]^{v-1} + \frac{y_s - x_s}{\sigma_n^2} = 0 \quad (15)$$

The evidence maximization algorithm is used in order to find the best model's parameters (v, θ) . The analytical solution for the integral over the posterior $p(y|x)p(x|\theta)$ does not exist; therefore, the evidence is approximated. The multidimensional pdf is approximated by the multivariate Gaussian distribution with Hessian matrix H centered on the maximum of the a posteriori distribution (Walessa & Datcu, 2000), (Sivia, 1996). The integral over a posterior pdf consists of mutually independent random variables; therefore, a conditional pdf can be rewritten as a product of their components

$$\begin{aligned} p(y|\theta) &= \int p(y|x)p(x|\theta) dx \\ p(y|\theta) &\approx \int \prod_{i=1}^N p(y_i|\hat{x}_i)p(\hat{x}_i|\theta) \exp\left(-\frac{1}{2}\Delta x^T H \Delta x\right) dx \\ p(y|\theta) &\approx \frac{(2\pi)^{N/2}}{\sqrt{|H|}} \prod_{i=1}^N p(y_i|x_i)p(x_i|\theta) \end{aligned} \quad (16)$$

where $\Delta x = x - \hat{x}$ and Hessian matrix H is a square matrix of the second-order partial derivatives of a univariate function

$$H = -\nabla \nabla \sum_{i=1}^N \log(p(y_i|x_i)p(x_i|\theta)) \quad (17)$$

The MAP estimate is computed using a numerical method. The texture parameters θ of the GGMRF model are estimated using the Minimum Mean Square Error (MMSE) estimation technique, and therefore given by a linear model as

$$\theta = (GG^T)^{-1} (G^T X) \tag{18}$$

where X are the observed coefficients inside the window of a size $N \times N$, and matrix G consists of neighboring coefficients attributed around each individual observed coefficient x_s inside a window of a size $N \times N$. The organization of a neighborhood for the bandelet and contourlet domain is shown in Fig. 9 and Fig. 10, respectively. Those figures show the parent-child relationships for the bandelet and contourlet transform. Each parameter θ weights the clique on different subbands.

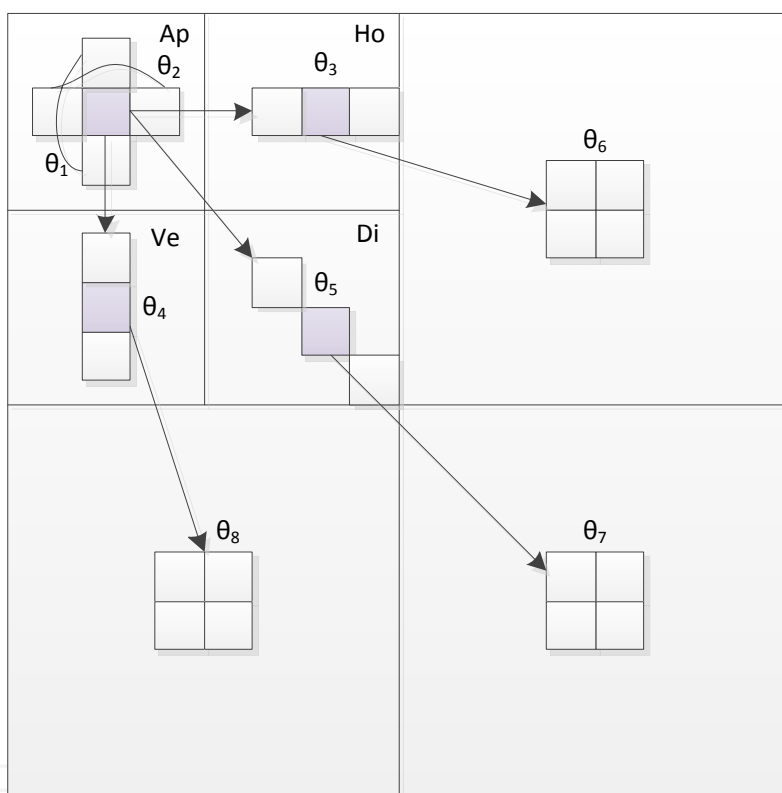


Fig. 9. Neighborhood cliques' organization for bandelet transforms

A logarithmic form can be introduced to simplify Eq. (16) as

$$\log p(y|x) \approx \sum_{i=1}^N \frac{1}{2} (\log(2\pi) - \log(h_{ii})) + \log p(y_i|\hat{x}_i) + \log p(\hat{x}_i|\theta) \tag{19}$$

where h_{ii} are the diagonal elements of the Hessian matrix H , which has dimensions of $N \times N$, and N represents the dimension of moving window. Another approximation is then made

$$|H| \approx \prod_{i=1}^N h_{ii} \tag{20}$$

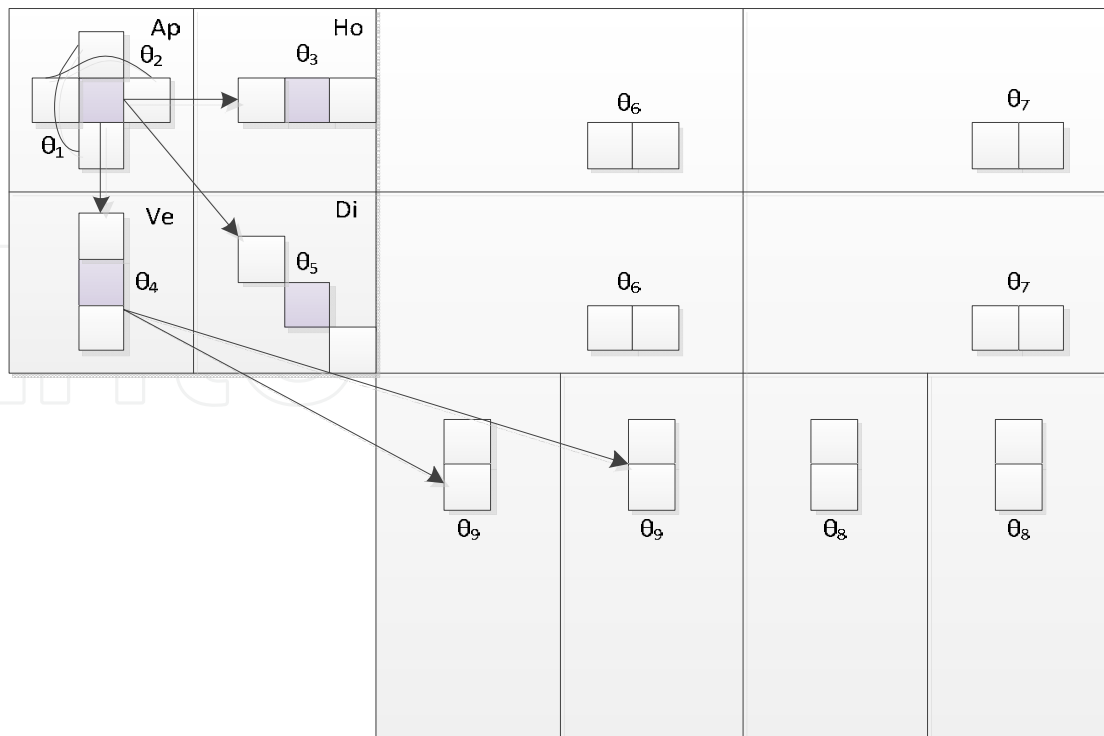


Fig. 10. Neighborhood cliques' organization for contourlet transforms

This approximation is possible, because all off-main diagonal elements represent covariances, and these are sparsely set matrixes that are close to zero, therefore those elements can be neglected. This assumption is in accordance with the statistical independence in Eq. (16). Only main-diagonal elements are needed for the Hessian matrix H , which are defined by

$$h_{ii} = \sum_{i=1}^N -v(v-1)\eta(v, \sigma_x)^2 \left(\eta(v, \sigma_x) \left| \hat{x}_i - \sum_{i \in \zeta} \theta_j (x_i^j + x_i^{j'}) \right| \right)^{v-2} - \sum_{i=1}^N \frac{\hat{x}_i}{\sigma_n^2} \quad (21)$$

4. Outline of the proposed algorithm

1. The proposed despeckling algorithm transforms SAR images using bandelet (Le Pennec & Mallat, Apr 2005) or contourlet (da Cunha et al., 2006) transform. The number of decompositions depends on the size of the image. The number of levels l is chosen in such a way that the size of the approximation subband is larger than or equal to 64×64 pixels (minimum size).
2. The model parameters v and θ are estimated inside a window with a size of $N \times N$ pixels. In all experiments, a window with 7×7 pixels was used.
3. The noise and signal variances are estimated using (13) and (14), respectively.
4. The parameter θ is estimated using the MMSE defined in (18).
5. The shape parameter v is changed within the interval $[0.5 \dots 2.5]$ with a step size of 0.1.
6. The noise-reduced coefficients are estimated using the MAP estimate (15) for each value v . Each time, the texture parameters θ are estimated using the MAP estimate obtained in the previous step.

7. The MAP estimate is used for the evidence estimation (21).
8. The best MAP estimate \hat{x} is accepted where the evidence has maximum value.
9. The algorithm proceeds to the next pixel.

5. Experimental results

5.1 Synthetic SAR images

The synthetic SAR image, shown in Fig. 11, is composed of four different areas and with added four-look multiplicative speckle noise. The SAR image size shown in Fig. 11 is 512×512 pixels; therefore three levels of decomposition are used for bandelet transform. First let us show the difference between the pure bandelet and contourlet, and the MBD method.

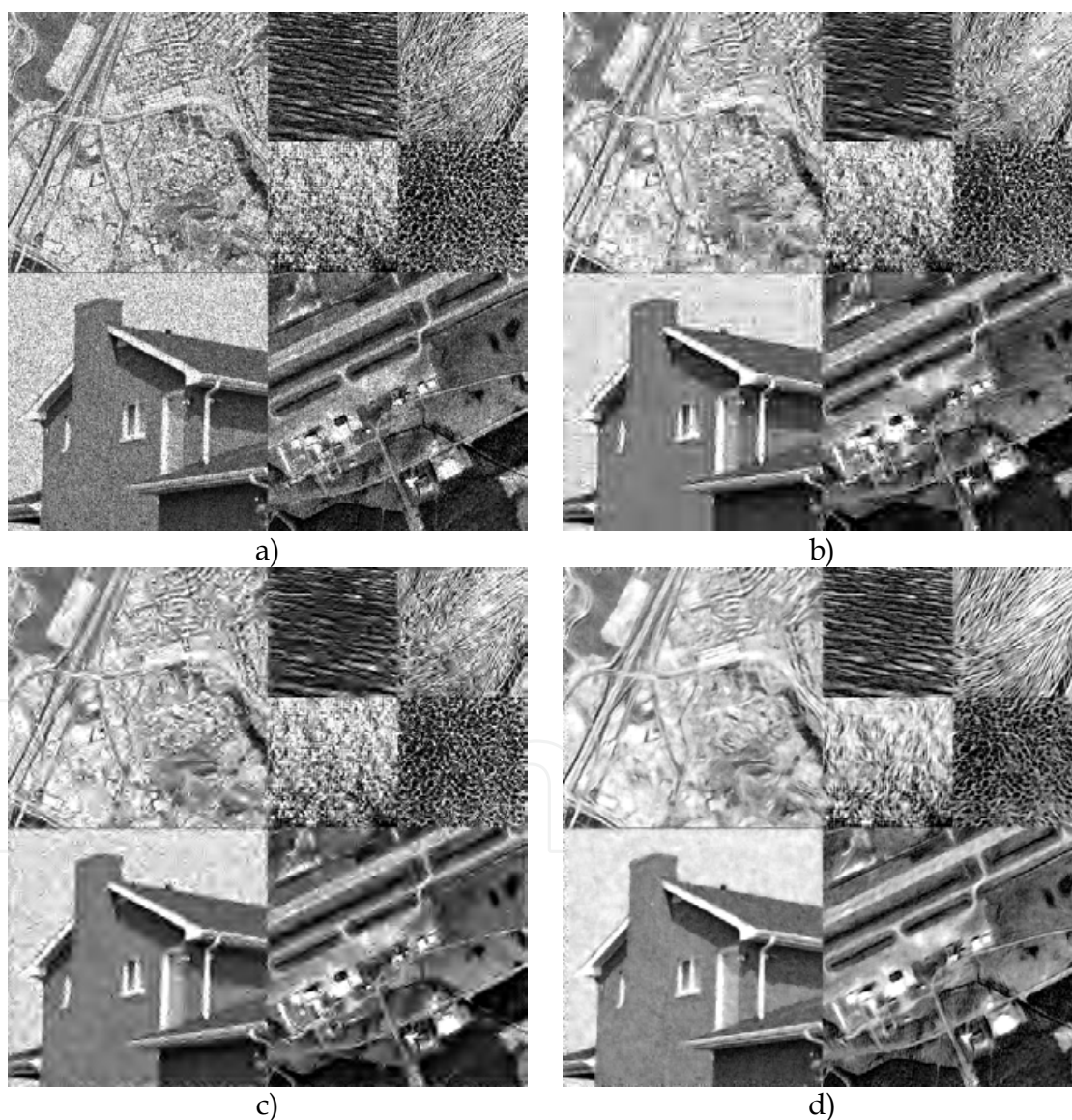


Fig. 11. a) Original speckled image, b) Despeckled image obtained with the original bandelet denoising scheme, c) Despeckled image obtained with the original contourlet denoising scheme, and d) Despeckled image obtained with the MBD denoising technique

The bandelet transform is composed of a larger sliding window with a size of 16×16 (i.e. moving window per window), meanwhile inside a larger window, a smaller one with the size of 4×4 pixels moves on pixel basis. Those two sliding windows are used for searching the best decomposition inside the dyadic wavelet transform (Le Pennec & Mallat, Apr 2005). The contourlet transform is constructed using eight directions at the first level of decomposition. The last two levels are chosen to be dyadic, but this is not a requirement. The despeckled images obtained using the bandelet and contourlet transform are shown in Fig. 11 b) and c), respectively. Moreover, the despeckled image obtained using the MBD (Walessa & Datcu, 2000) is shown in Fig. 11 d).

And now with the MAP incorporated into the bandelet and contourlet transform.

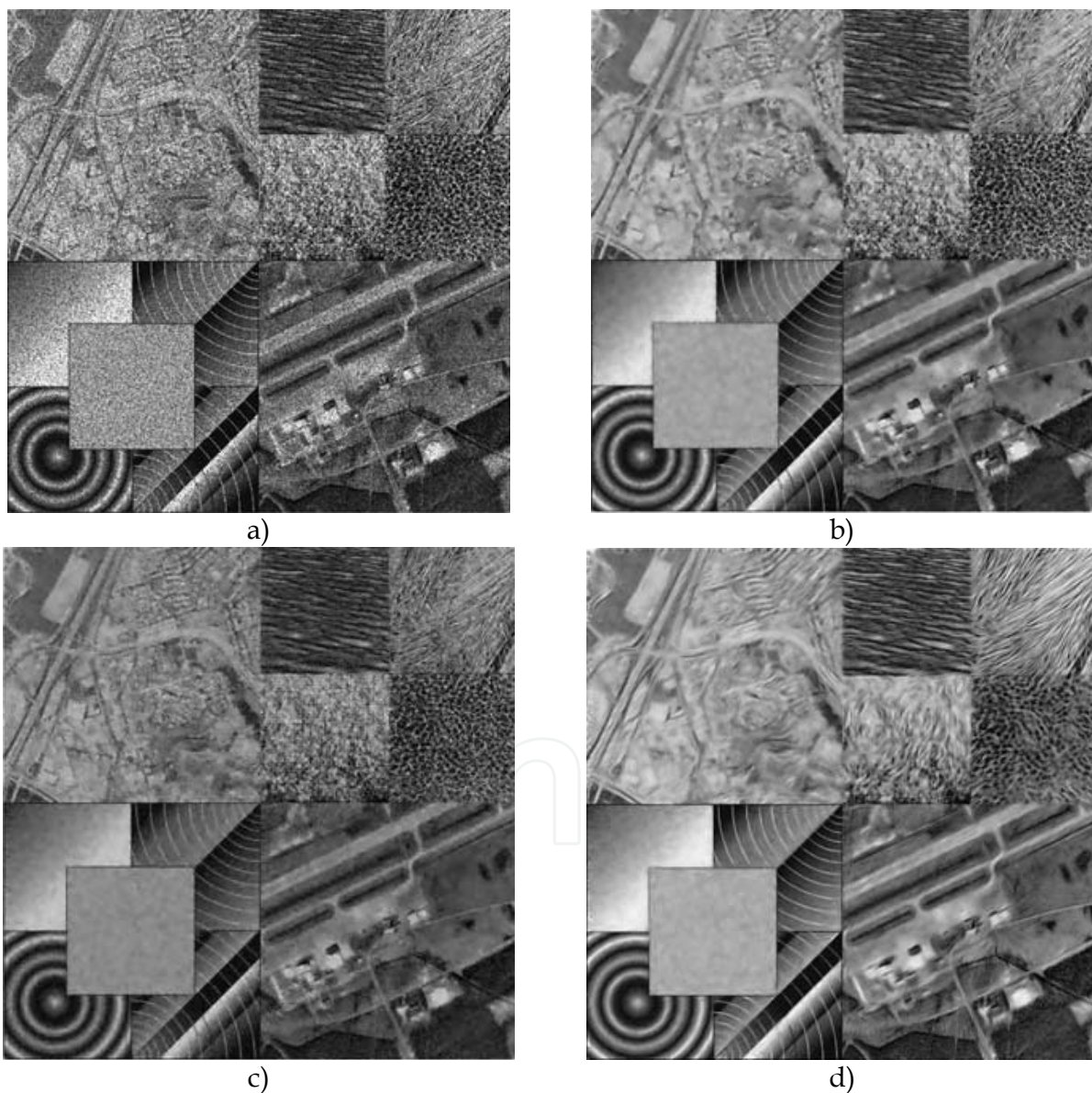


Fig. 12. a) Original speckled image, b) Despeckled image obtained with the bandeleted denoising scheme, c) Despeckled image obtained with the contourlet denoising scheme, and d) Despeckled image obtained with the MBD denoising technique

$\mu = 127.94$	<i>Bandelet</i>	<i>Contourlet</i>	<i>MBD</i>
MSE	331	447	463
Mean	127.64	127.4	126.49
ENL (\hat{x})	506	510	539
ENL (y/\hat{x})	3.14	3.2	3.18
Mean (y/\hat{x})	1.047	1.048	0.94

Table 1. Filter evaluation for synthetic test images

In Table 1, the objective measurements are presented for the denoising of image shown in Fig. 12. Objective measurements include the mean-square error (MSE), the equivalent number of looks (ENL), the mean value of the despeckled image, the ENL of speckle noise ($ENL(y/\hat{x})$), and the mean value of speckle noise y/\hat{x} . The ENL of the image is given by μ^2/σ^2 . The best MSE results are from bandelet transform in combination with Bayesian inference, thus having better results than those obtained from the contourlet transforms. A drawback of the contourlet transform is that it produces contours in the reconstructed image, which affects a MSE value. All wavelet-based methods well preserve the mean of the despeckled images. On the other hand, the MBD method well estimates the speckle noise, but it overblurs the reconstructed image, yielding a worse MSE value.

Figs. 13 a)-c) show the ratio images between the original and the reconstructed mosaic images obtained with bandelet, contourlet, and MDB. From these ratio images we can conclude that edges are well preserved, and that the speckle noise in the homogeneous areas is well estimated (i.e. removed) using the MBD method and second generation wavelets, as reported in Table 1.

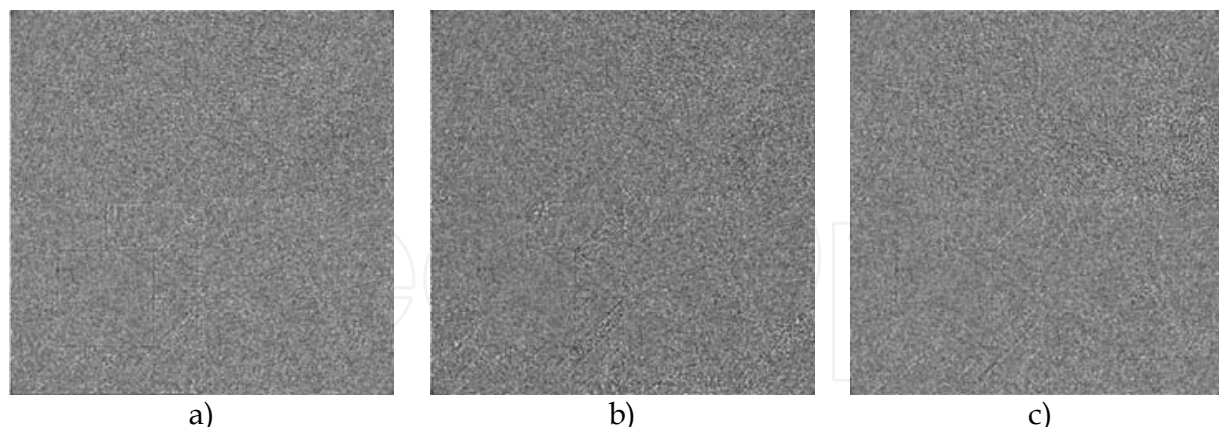


Fig. 13. Ratio images y/\hat{x} . a) Ratio image obtained with the bandelet-based despeckling, b) Ratio image obtained with the countourlet-based despeckling, and c) Ratio image obtained with the MBD method

The efficiency of the texture separation regarding the proposed method is demonstrated on four Brodatz textures, which are presented in a single mosaic composition and shown in Fig. 14. The textures are corrupted with a four-look speckle noise. The estimated parameter θ_2 obtained from bandelet and contourlet transforms is shown in Fig. 14 b) and

c), respectively. The estimated texture parameters θ are classified into four classes using the K -means algorithm, and the classification results are shown in Fig. 14 d) and e), respectively. The best texture separation is obtained using a contourlet transform. The unsupervised classification of the texture parameters has an accuracy rate of 82 % and 89 %, for texture parameters obtained from the bandelet and contourlet transforms, respectively. Fig. 14 f) shows the classification of the texture parameter θ obtained with the MBD method. This method cannot well estimate classes on the right side of the image shown in Fig. 14 f).

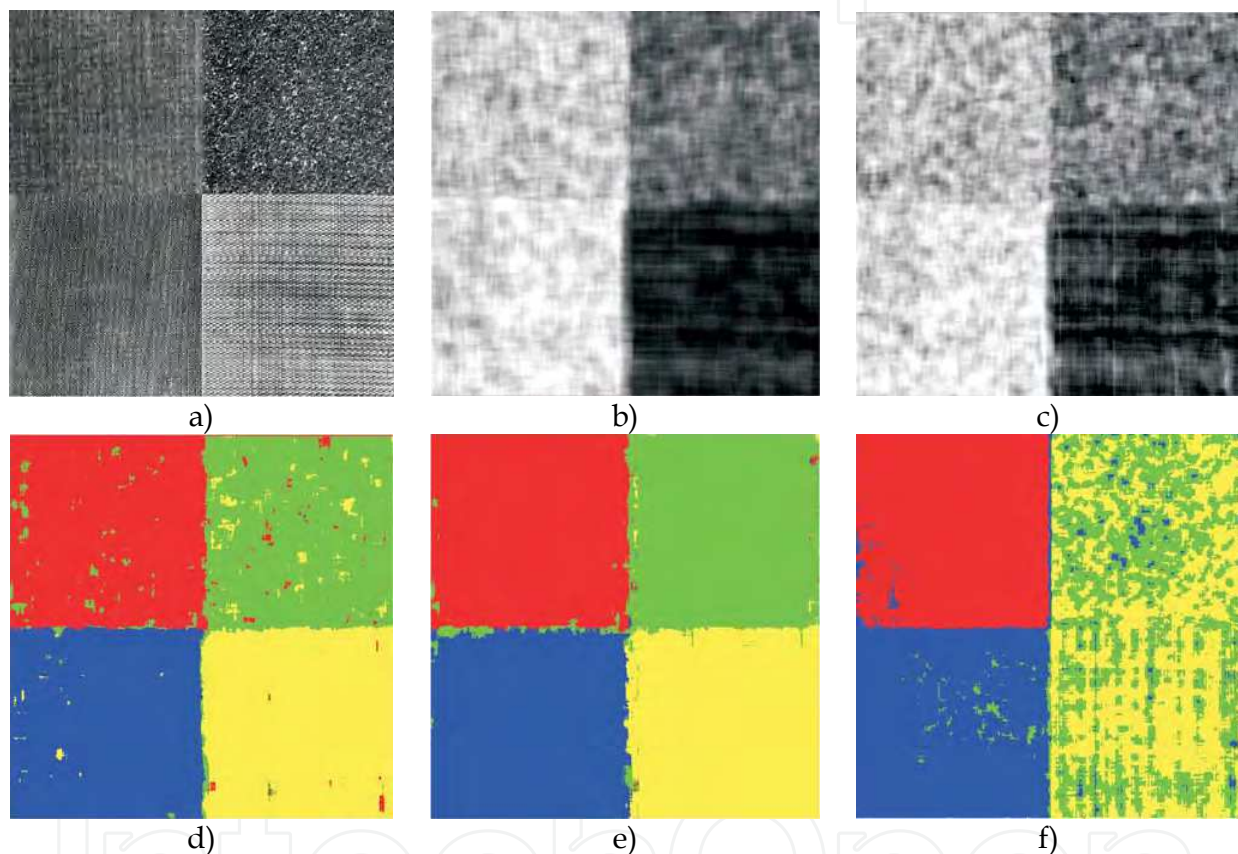


Fig. 14. a) Brodatz textures composed into a mosaic image, b) Texture parameter θ_2 obtained with the bandelet transform, c) Texture parameter θ_2 obtained with the contourlet transform, d) Classified parameter θ obtained with the bandelet transform using the K -means unsupervised classification into four classes, e) Classified parameter θ obtained with the contourlet transform using the K -means unsupervised classification into four classes, and f) Classified parameter θ obtained with the MBD method and K -means unsupervised classification into four classes

5.2 Real SAR images

The real SAR images are a sample images taken by TerraSAR-X satellite. The amplitude part of a single-look complex (SLC) SAR image is shown in Fig. 15 with a size of 2048×2048 pixels and ENL equal to 1.1. Four levels of dyadic decomposition are used for the bandelet

decomposition. Five levels of contourlet transform are used, where the last two decompositions are dyadic and all other levels are contourlet directional subbands consisted of eight directional subbands. The Daubechies symmetric four-filter bank (Daubechies, 1992) is used for the construction of bandelet and contourlet transforms.



a)



b)



c)



d)

Fig. 15. a) Original TerraSAR-X image © DLR (2007), b) Despeckled image obtained with the bandelet transform, c) Despeckled image obtained with the contourlet transforms, and d) Despeckled image obtained with the MBD method

Fig. 15 a)-d) shows the original SLC SAR image and the despeckled images obtained using the bandelet- and contourlet-based despeckling techniques, and the MBD despeckling method. Their ratio images are shown in Fig. 16 a)-c). The quality of the reconstructed images using the bandelet and contourlet transforms is nearly the same. However, the despeckling method based on bandelet transform has left out some speckle noise in the homogeneous regions. On the other hand, the homogeneous regions are well despeckled in the reconstructed image based on the contourlet transform, but undesired artifacts emerge in places around strong scatter returns in shape of lines, that are a consequence of contourlet subbands decomposition. This artifact is clearly visible in Fig. 16 b). Figs. 17 a)-c) show how strong scatterers are despeckled within the bandelet, contourlet, and dyadic wavelet domain.

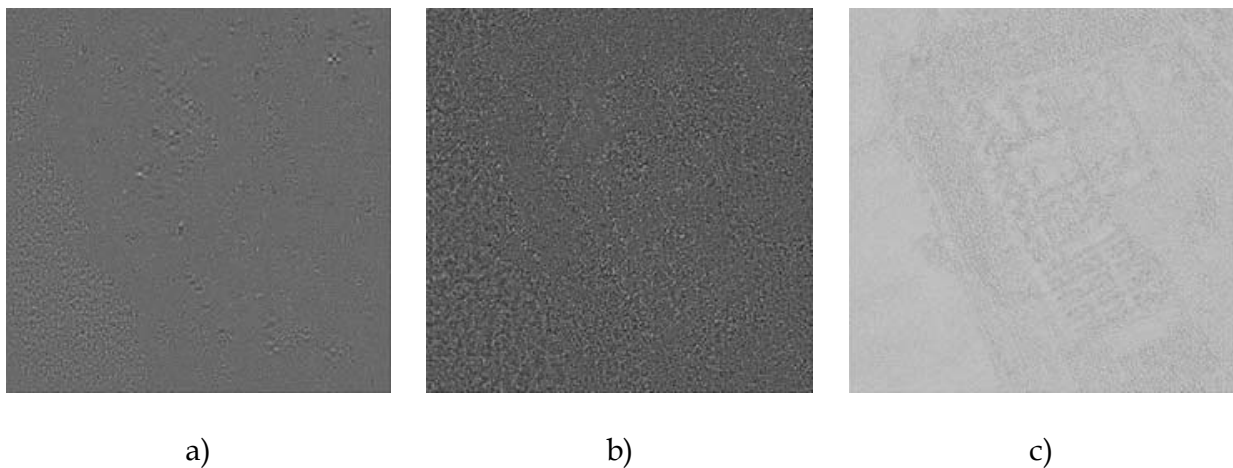


Fig. 16. Ratio images y/\hat{x} for SAR images. a) Ratio image obtained with the bandelet transform, b) Ratio image obtained with contourlet transform, and c) Ratio image obtained with the MBD method

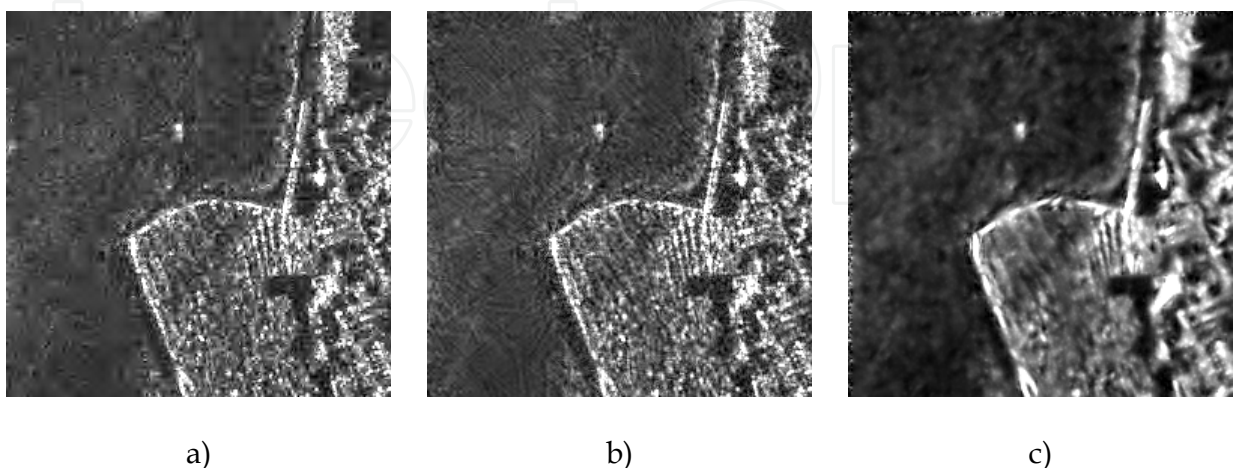


Fig. 17. Despeckling of strong scatterers using a) bandelet transform, b) contourlet transform, and c) MBD method

The despeckling within the bandelet and dyadic wavelet domain are able to remove speckles around the strong scatterers, while the contourlet transform produces artifacts in this configuration. Higher image values are difficult to despeckle, because of the nature of the contourlet transform. Therefore, the noise is still present in those areas of the reconstructed image. However, the bandelet transform is overall computationally more demanding than contourlet transform (around 5.6 times), yet the despeckling of each contourlet subband takes about 4.5 times longer than with bandelet transform. Therefore, these methods are also computationally comparable.

To extract texture information from the denoised TerraSAR-X images we have used General Gauss-Markov Random Fields (GGMRF) as a prior pdf (Gleich & Datcu, 2007). As a prior pdf a first order model was used with cliques defined as Gauss-Markov Random Fields and shown in Figs. 9 and 10. Cliques were used to estimate central pixels for both transforms created in a 7×7 window which is moving throughout the whole picture. This was applied on transform's first approximation and its corresponding subbands. The texture parameters are iteratively estimated until second order Bayesian inference is increasing, which is used for finding the best model (Gleich & Datcu, 2007). The results of this method can be seen in Fig. 18, where the classification parameters for *K*-means algorithm were 5 classes and 7 iterations.

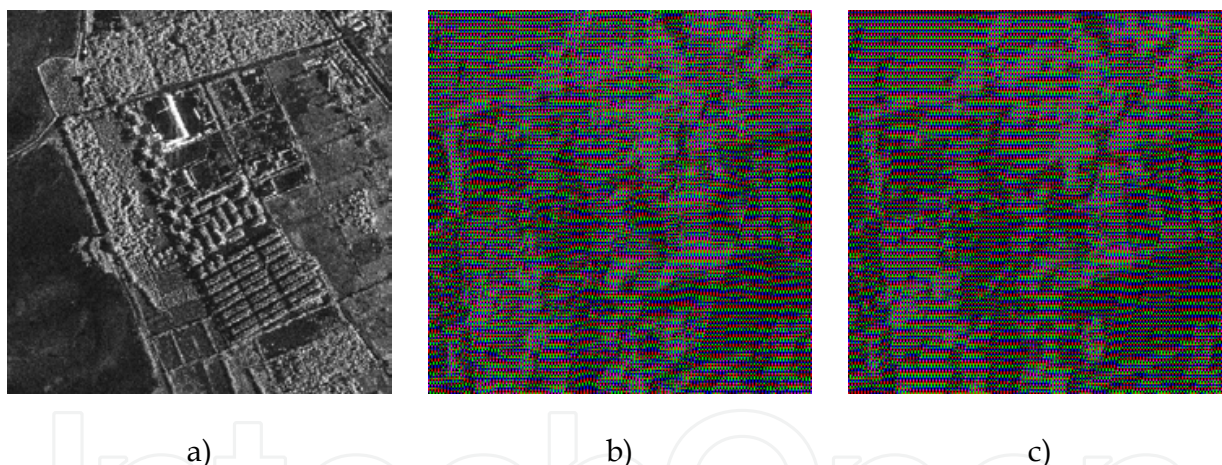


Fig. 18. Comparison on information extraction. A) Original TerraSAR-X© image, b) Classified image on bandelet transform subbands, and c) Classified image on contourlet transform subbands

Texture parameters θ obtained during the despeckling procedure of the SAR image shown in Fig. 15 with bandelet, contourlet, and MBD method are shown in Fig. 19 b)-d). The algorithm used for classification into four different classes is the *K*-means algorithm. Fig. 19 a) is an indication of *K*-means algorithm applied to original image scene, where no textures can be identified as no processing was applied. The texture parameters obtained with both proposed algorithms clearly separate between homogeneous and heterogeneous areas. The contourlet transform compared to bandelet transform better separates the homogeneous and heterogeneous areas. From images it can be concluded, that contourlet transform is able to separate more heterogeneous areas from homogeneous ones. As a comparison, the MBD

method can also distinct between homogeneous and heterogeneous areas as well as separate different textures in the scene, as shown in Fig. 19 d).

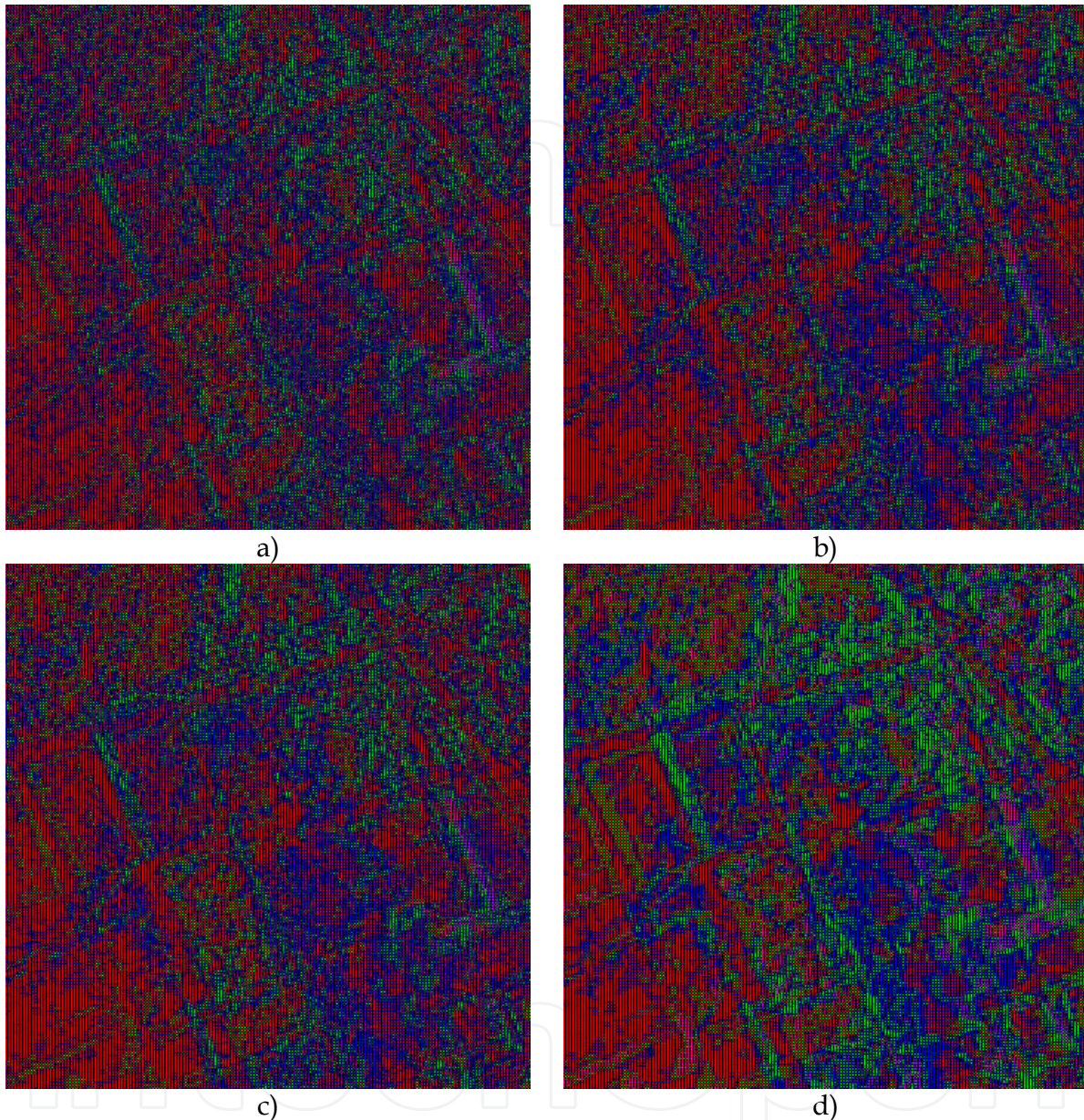


Fig. 19. Classification of texture parameter θ using the K-means algorithm and the a) original, b) bandelet, c) contourlet, and d) MBD-based algorithm

6. Conclusion

This book chapter has presented the proposed methods for despeckling a synthetic and real SAR images using second-generation wavelets. The Bayesian approach is incorporated into second generation wavelets using the wavelet domain. The prior and likelihood pdfs are modeled using GGMRF and Gaussian distribution. The second order Bayesian inference is used to better estimate model parameters and to find the best values possible. The evidence

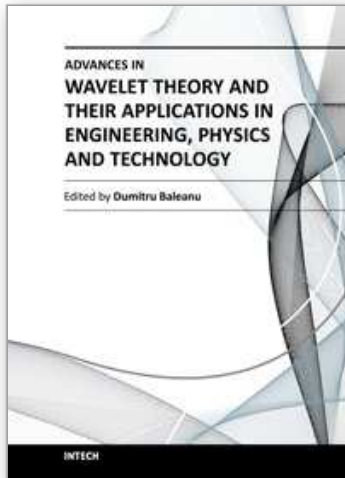
has been simplified and approximated using the Hessian approach. The experimental results have shown that the despeckling of real SAR images using second-generation wavelets is comparable with the dyadic wavelet-based despeckling algorithm (Gleich & Datcu, 2006). Moreover, information extracted using the contourlet domain gives good results using synthetic as well as real SAR data. Unfortunately, the contourlet-based despeckling introduces lines, which are consequences of cutting low-frequency components in the subband decomposition, which can be corrected by introducing a new filter or by post-processing step.

7. References

- Argenti, F., and Alparone L. (2002). Speckle Removal From SAR Images in the Undecimated Wavelet Domain. *IEEE Tran. Geoscience and Remote Sensing*, Vol. 40, No. 11, (November 2002), pp. 2363-2374
- Bamberger, R. H., and Smith, M. J. T. (1992). A filter bank for the directional decomposition of images: Theory and design. *IEEE Trans. Signal Proc.*, Vol. 40, No. 4, (April 1992), pp. 882-893
- Chuna, A. L., Zhou, J. and Do, M. N. (2006). The Nonsubsampled Contourlet Transform: Theory, Design, and Application. *IEEE Tran. Image Processing*, Vol. 15, No. 10, (October 2006), pp. 3089-3101
- Cui, J., and Wong W. (2006). Adaptive Chirplet Transform and Visual Evoked Potentials. *IEEE Tran. on Biomedical Engineering*, Vol. 53, No. 7, (July 2006), pp. 1378-1384
- da Cunha, A. L., Zhou, J., and Do, M. N. (2006). The Nonsubsampled Contourlet Transform: Theory, Design, and Applications. *IEEE Transactions on Image Processing*, Vol. 15, No. 10, (October 2006), pp. 3089-3101
- Dai, M., Cheng, P., Chan, A. K., and Loguinov D. (2004). Bayesian Wavelet Shrinkage with Edge Detection for SAR Image Despeckling. *IEEE Tran. Geoscience and Remote Sensing*, Vol. 42, No. 8, (August 2004), pp. 1642-1648
- Daubechies, I. (June 1, 1992). *Ten Lectures on Wavelets* (1st edition), SIAM: Society for Industrial and Applied Mathematics, 978-0898712742, Philadelphia, Pennsylvania
- Do, M. N. and Vetterli, M. (2005). The Contourlet transform: an efficient directional multiresolution image representation. *IEEE Trans. Image Process.*, Vol. 14, No. 12, (December 2005), pp. 2091-2106
- Foucher, S., Benie, G. B., and Boucher, J. M. (2001). Multiscale MAP filtering of SAR Images. *IEEE Tran. Image Processing*, Vol. 10, No. 1, (January 2001), pp. 49-60
- Frost, V. S., Stiles J. A., Shanmugan K. S., and Holtzman J. C. (1982). A model for radar images and its application to adaptive digital filtering of multiplicative noise. *IEEE Trans. Pattern Anal. Mach. Intell.*, Vol. 4, No. 2, (February 1982), pp. 157-166
- Gleich, D., and Datcu, M. (2006). Gauss-Markov Model for SAR image Despeckling. *IEEE Signal Processing Letters.*, Vol. 13, No. 6, (June 2006), pp. 365-368
- Gleich, D., and Datcu, M. (2007). Wavelet-Based Despeckling of SAR Images Using Gauss-Markov Random Fields. *IEEE Transactions on Geoscience and Remote Sensing*, Vol. 45, No. 12, (December 2007), pp. 4127-4143
- Kuan, D. T., Sawchuk A. A., Strand T. C., and Chavel P. (1985). Adaptive noise smoothing filter for images with signal-dependent noise. *IEEE Trans. Pattern Anal. Mach. Intell.*, Vol. 7, No. 2, (February 1985), pp. 165-177

- Le Pennec, E., and Mallat, S. (2001). Bandelet Image Approximation and Compression. In Proc. Int. Conf. Image Processing, ISBN: 0-7803-6725-1, Thessaloniki, Greece, October 2001
- Le Pennec, E., and Mallat, S. (2005). Bandelet Image Approximation and Compression. *SIAM Journ. of Multiscale Modeling and Simulation*, Vol. 4, No. 3, (December 2005), pp. 992-1039
- Le Pennec, E., and Mallat, S. (2005). Sparse geometric image representations with bandelets. *IEEE Transaction on Image Processing*, Vol. 14, No. 4, (April 2005), pp. 423-438
- Lee, J. S. (1980). Digital image enhancement and noise filtering by use of local statistics. *IEEE Trans. Pattern Anal. Machine Intell.*, Vol. 2, No. 2, (March 1980), pp. 165-168
- Li, Y., He, M. and Fang, X. (2006). A New Adaptive Algorithm for Despeckling of SAR images Based on Contourlet Transform. *IEEE Conference on Signal Processing*, ISBN 0-7803-9736-3, Guilin, China, November 2006
- Peyré, G., and Mallat, S. (2005). Surface compression with geometric bandelets. *ACM Transactions on Graphics*, Vol. 24, No. 3, (July 2005), pp. 601-608
- Sivia, D. S. (September 26, 1996). *Data Analysis: A Bayesian Tutorial* (1st edition), Oxford University Press, 978-0198518891, USA
- Sveinsson, J. R., Semar Z., and Benediktsson, J. A. (2008). Speckle Reduction of SAR Images in the Bandelet Domain. *IEEE International Conference on Geoscience and Remote Sensing*, ISBN: 978-1-4244-2807-6, Boston, MA, July 2008
- Vetterli, M. (1984). Multi-dimensional subband coding: some theory and algorithms. *Signal Processing*, Vol. 6, No. 2, (April 1984), pp. 97-112
- Walessa, M., and Datcu M. (2000). Model-Based Despeckling and Information Extraction from SAR images. *IEEE Tran. Geoscience and Remote Sensing*, Vol. 38, No. 5, (September 2000), pp. 2258-2269
- Wikipedia. (18 January 2011). TerraSAR-X, In: *Wikipedia*, October 6 2011, Available from: <http://en.wikipedia.org/wiki/TerraSAR-X>
- Yang, S., Liu, F., Wand, M., and Jiao, L. (2007). Multiscale bandelet image compression. *International Symposium on Intelligent Signal Processing and Communication Systems*, ISBN 978-1-4244-1447-5, Xiamen, November 2007

IntechOpen



Advances in Wavelet Theory and Their Applications in Engineering, Physics and Technology

Edited by Dr. Dumitru Baleanu

ISBN 978-953-51-0494-0

Hard cover, 634 pages

Publisher InTech

Published online 04, April, 2012

Published in print edition April, 2012

The use of the wavelet transform to analyze the behaviour of the complex systems from various fields started to be widely recognized and applied successfully during the last few decades. In this book some advances in wavelet theory and their applications in engineering, physics and technology are presented. The applications were carefully selected and grouped in five main sections - Signal Processing, Electrical Systems, Fault Diagnosis and Monitoring, Image Processing and Applications in Engineering. One of the key features of this book is that the wavelet concepts have been described from a point of view that is familiar to researchers from various branches of science and engineering. The content of the book is accessible to a large number of readers.

How to reference

In order to correctly reference this scholarly work, feel free to copy and paste the following:

Matej Kseneman and Dušan Gleich (2012). Information Extraction and Despeckling of SAR Images with Second Generation of Wavelet Transform, *Advances in Wavelet Theory and Their Applications in Engineering, Physics and Technology*, Dr. Dumitru Baleanu (Ed.), ISBN: 978-953-51-0494-0, InTech, Available from: <http://www.intechopen.com/books/advances-in-wavelet-theory-and-their-applications-in-engineering-physics-and-technology/information-extraction-and-despeckling-of-sar-images-with-second-generation-of-wavelet-transform>

INTECH
open science | open minds

InTech Europe

University Campus STeP Ri
Slavka Krautzeka 83/A
51000 Rijeka, Croatia
Phone: +385 (51) 770 447
Fax: +385 (51) 686 166
www.intechopen.com

InTech China

Unit 405, Office Block, Hotel Equatorial Shanghai
No.65, Yan An Road (West), Shanghai, 200040, China
中国上海市延安西路65号上海国际贵都大饭店办公楼405单元
Phone: +86-21-62489820
Fax: +86-21-62489821

© 2012 The Author(s). Licensee IntechOpen. This is an open access article distributed under the terms of the [Creative Commons Attribution 3.0 License](#), which permits unrestricted use, distribution, and reproduction in any medium, provided the original work is properly cited.

IntechOpen

IntechOpen